PCCP

PAPER

View Article Online
View Journal | View Issue

Cite this: *Phys. Chem. Chem. Phys.*, 2014, **16**, 1667

Mechanical and electronic properties of pristine and Ni-doped Si, Ge, and Sn sheets

Aaditya Manjanath,[ab] Vijay Kumar[cd] and Abhishek K. Singh*[a]

Received 4th November 2013,
Accepted 18th November 2013

DOI: 10.1039/c3cp54655a

www.rsc.org/pccp

Silicene, a graphene analogue of silicon, has been generating immense interest due to its potential for applications in miniaturized devices. Unlike planar graphene, silicene prefers a buckled structure. Here we explore the possibility of stabilizing the planar form of silicene by Ni doping using first principles density functional theory based calculations. It is found that planar as well as buckled structure is stable for Ni-doped silicene, but the buckled sheet has slightly lower total energy. The planar silicene sheet has unstable phonon modes. A comparative study of the mechanical properties reveals that the in-plane stiffness of both the pristine and the doped planar silicene is higher compared to that of the buckled silicene. This suggests that planar silicene is mechanically more robust. Electronic structure calculations of the planar and buckled Ni-doped silicene show that the energy bands at the Dirac point transform from linear behavior to parabolic dispersion. Furthermore, we extend our study to Ge and Sn sheets that are also stable and the trends of comparable mechanical stability of the planar and buckled phases remain the same.

Graphene has attracted great attention and has created much excitement about the possible technological applications due to its unusual electronic properties arising from the sp^2 hybridized planar structure.[1] However, a direct industrial application of graphene in devices is yet to be achieved, because it would require development of a different infrastructure than currently available. On the other hand silicon based nanostructures are very desirable for miniature devices as one can take advantage of the existing facilities of widely used silicon electronic devices. Recently, a graphene analogue, named silicene, has been synthesized on ZrB_2(0001) thin films[2] and the Ag(110) substrate.[3,4] Its band structure shows linear dispersion near the *K*-point (a property that made graphene so attractive), but it prefers a buckled honeycomb structure.[2–7] Further, similar to silicene, pristine Ge sheets have been shown to also favor a buckled configuration.[5–7]

Nanostructures of pristine silicon and other group IV elements such as Ge and Sn do not have the versatility of structures in low dimensions as those of carbon such as the formation of fullerenes and nanotubes. However, by doping transition metal (TM) atoms, one can form a family of highly symmetric structures of silicon such as metal-encapsulated fullerenes and other polyhedral forms as well as nanotubes. Extensive theoretical and experimental studies[8–14] have shown stabilization of highly symmetric endohedral structures $TM@X_n$, where X = Si, Ge, Sn, and Pb. The TM atom gets encapsulated inside a cage whose size in general depends on the metal atom as well as X atoms and may be in between $20 \geq n \geq 8$.[15] Furthermore, some clusters display very large HOMO–LUMO gaps[8–10,12,13] and magnetic moments,[11,14] suggesting their possible applications in the field of optoelectronics and spintronics. In recent years stable metal-encapsulated magic clusters of the form $X_{10}M$ (where M = Ni, Pd or Pt)[16,17] have been successfully produced in large quantity.

In 2002, even before the advent of graphene in laboratory, Singh *et al.* showed that the 0-dimensional Be-encapsulated clusters could be assembled to form 1-dimensional nanotubes[18,19] in which metal atoms stabilize silicon in sp^2 bonding configuration. Further, it was shown that hexagonal Si nanotubes could be stabilized using 3d transition metals (TM).[20] These nanotubes have a stacking of hexagonal rings with the metal atoms sandwiched between the hexagons. The distance between the metal atom and the center of the hexagon changes with the type of the metal atoms. In the case of Ni, this distance goes to zero, and it lies at the center of the hexagonal rings. It is therefore interesting to explore if such hexagonal rings with Ni at the center can be attached sideways to form a planar 2D-sheet. Note that nickel silicide is an important material for silicon devices. Here, using first principles density functional calculations, we show that a planar as well as a buckled sheet of Si can be stabilized by Ni doping. The planar sheets, however, have unstable phonon modes, but they exhibit better in-plane stiffness compared with the buckled sheets. The electronic structure calculations show that the linear dispersion of the

[a] *Materials Research Centre, Indian Institute of Science, Bangalore 560012, India. E-mail: abhishek@mrc.iisc.ernet.in*
[b] *Centre for Nano Science and Engineering, Indian Institute of Science, Bangalore 560012, India*
[c] *Dr Vijay Kumar Foundation, 1969, Sector 4, Gurgaon 122 001, Haryana, India*
[d] *Center for Informatics, School of Natural Sciences, Shiv Nadar University, Chithera, Gautam Budh Nagar 203 207, Uttar Pradesh, India*

bands at the Dirac point transforms to parabolic type upon doping with Ni. The doped sheets have improved metallicity (finite density of states at the Fermi level) compared with the pristine sheets. Similar to the case of Si, Ge nanotubes have also been stabilized using TM atoms.[21,22] Besides stabilizing them, the TM atoms make the Ge nanotubes semiconducting.[23,24] Motivated by this work, we extend our study to Ge and Sn sheets as well. Our results show that Ni-doped Ge sheets show unstable modes for both the buckled as well as planar cases, whereas, Sn follows the same trend as silicene. Further, we have studied the effect of dopants such as Fe and Co on the properties of silicene and compared them with those of Ni.

The electronic structure calculations have been performed using first-principles density functional theory (DFT).[25] Projector augmented wave (PAW)[26,27] pseudopotentials were used to represent the electron–ion interactions. The exchange and correlation part of the total energy is approximated by the generalized gradient approximation (GGA) using Perdew–Burke–Ernzerhof type of functional[28] as implemented in Vienna Ab initio Simulation Package (VASP).[29,30] A primitive cell configuration of two atoms was used for all the sheets, with a vacuum of 15 Å along the z-axis (Fig. 1) to avoid spurious interactions between the periodic images. Calculations with a larger supercell yielded the same results. For integrations over the Brillouin zone, a dense Monkhorst–Pack k-point mesh[31] of $15 \times 15 \times 1$ was used. Structural relaxation was performed using the conjugate-gradient method until the absolute value of the Hellman–Feynman forces were converged to within 0.005 eV Å^{-1}. Spin-polarized calculations were performed for Ni-doped sheets. Phonon dispersions were obtained by using density functional perturbation theory (DFPT).[32] An energy cutoff of 600 eV and a convergence criterion of 1×10^{-8} eV were used to obtain high quality forces.

The structural parameters of the optimized planar as well as buckled sheets of both Ni-doped and pristine Si, Ge, and Sn are given in Table 1. The lattice parameter (a) and buckling height (δ) of pristine Si and Ge sheets are in good agreement with the earlier reported results.[5,6,33] In the case of pristine planar and buckled sheets, the bond length increases from Si to Sn due to the increase in the atomic radius. However, the increase in the bond length in the doped buckled sheets is much higher. The buckling height, defined as the deviation of the group-IV atoms from the plane, also increases from Si to Sn. This trend is in line with the behavior in bulk where the buckling heights observed for Si, Ge and Sn are 1.36 Å, 1.41 Å, and 2.06 Å, respectively. This is due to the increase in the bond length from Si to Sn. The buckling in the case of bulk structures is more than in sheets suggesting that the type of hybridization in sheets is not exactly sp^3 but of the type sp^2–sp^3. The buckling is more prominent in the case of the doped sheets. This indicates that upon Ni doping, Si prefers a configuration which is more towards the sp^3 hybridization. This tendency leads to less overlap among the p_z orbitals of group-IV atoms, which causes higher buckling. A similar trend is also observed for the equilibrium lattice parameters from Si to Sn, for both the pristine and the doped planar and buckled sheets. The buckled sheets have lower energy than the planar sheets and are therefore energetically more stable. The difference between the total energies of the planar and the buckled sheets ΔE increases from Si to Sn. There is a substantial increase in the value of ΔE in the case of the doped sheets. Furthermore, like Ni doped Si nanotubes, the magnetic moments are completely quenched[20] in all the sheets.

Table 1 Optimized structural parameters of pristine and Ni-doped 2D-sheets of Si, Ge, and Sn. The energies and lengths are given in eV and Å, respectively

	Planar		Buckled			
System	a	IV–IV bond length	a	IV–IV bond length	δ	ΔE
Si	3.9	2.25	3.9	2.29	0.43	0.03
Ge	4.1	2.39	4.1	2.48	0.67	0.05
Sn	4.8	2.77	4.8	2.88	0.80	0.28
Si@Ni	4.0	2.31	4.0	2.51	0.99	0.45
Ge@Ni	4.4	2.54	4.2	2.74	1.28	0.78
Sn@Ni	4.9	2.83	4.7	3.07	1.43	0.89

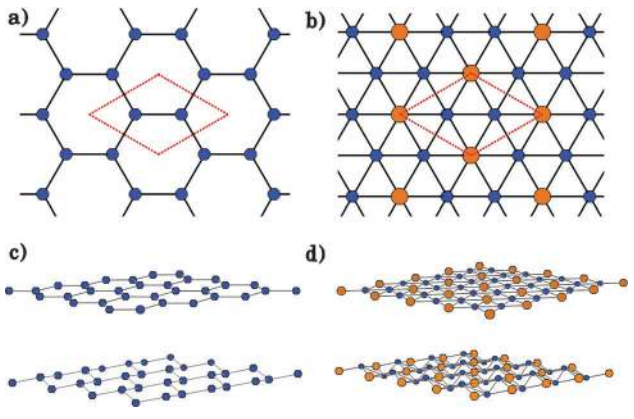

Fig. 1 (a) and (b) are the top views of optimized structures of pristine and Ni-doped silicene. (c) and (d) are the corresponding side views of planar and buckled sheets. Orange and blue color balls represent Ni and Si, respectively. The geometries of Ge and Sn sheets are similar.

Further, we studied the mechanical stability of the sheets from the point of view of their applications. This is characterized by the in-plane stiffness C which is a measure of the strength of the sheets. We computed C by applying a homogeneous strain ε on the sheets and it is given by:

$$\varepsilon = \frac{a - a_0}{a_0} \tag{1}$$

where a is the lattice constant with strain and a_0 the equilibrium lattice constant (no strain).

The energy E of a sheet around the equilibrium is given by the following Taylor series expansion upto 2nd order:

$$E = E_0 + \sum_{\alpha} \frac{\partial E}{\partial u_\alpha} u_\alpha + \sum_{\alpha,\beta} \frac{1}{2} \frac{\partial^2 E}{\partial u_\alpha \partial u_\beta} u_\alpha u_\beta + O\left(u^3\right) \tag{2}$$

where, u_α is the displacement of atoms along the αth direction and E_0 is the equilibrium energy. When written in terms of the

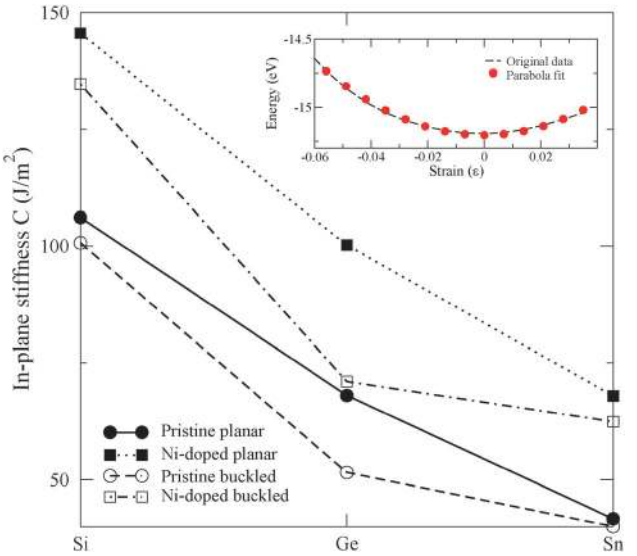

Fig. 2 The in-plane stiffness of planar and buckled pristine and Ni-doped sheets. The figure in the inset shows the parabola fit to the energy *vs.* strain plot for Ni-doped planar silicene case, to obtain the in-plane stiffness value. Similar are the plots for the other cases.

applied strain, the second derivative term of this equation gives us the value of C,[34] *i.e.*:

$$C = \frac{1}{A_0}\frac{\partial^2 E}{\partial \varepsilon^2} \quad (3)$$

where A_0 is the equilibrium area of the sheet. The total energy is calculated as a function of the strain. The data points are fitted to an equation of a parabola of the form[34] (inset of Fig. 2) $E = \frac{1}{2}\tilde{C}\varepsilon^2$, where $\tilde{C}$ is the fitting parameter and the in-plane stiffness C is given by: $C = \frac{\tilde{C}}{a_0^2}$. Fig. 2 shows a plot of in-plane stiffness of each sheet. For both the pristine and the doped cases, planar sheets have considerably higher C values than the buckled sheets because the sp^2 hybridized bonding in the planar sheets is stronger compared to sp^2–sp^3 hybridized bonding of the buckled sheets. This makes planar sheets mechanically stronger. Ni-doped sheets have larger C values than the pristine sheets indicating that doping these sheets with Ni reinforces their strength. Table 1 shows that ΔE values are very high for the doped sheets than the pristine sheets. This indicates that Ni stabilizes both planar as well as buckled sheets. However, unlike ΔE, C decreases from Si to Sn. This is due to the increasing tendency of metallic bonding in going from Si to Sn. This is also evident from the increase in the bond length from Si to Sn (Table 1).

Although, Ni-doped planar and buckled sheets are metastable, it is necessary to find any instabilities in the structures. The phonon dispersions of all the sheets have been calculated and have been shown for Si in Fig. 3. Similar to the pristine sheets[6,7] (Fig. 3(a)), planar doped sheets show strong instabilities as one of the acoustic modes exhibits negative frequencies (Fig. 3(c)). However, doped buckled sheets do not show these unstable

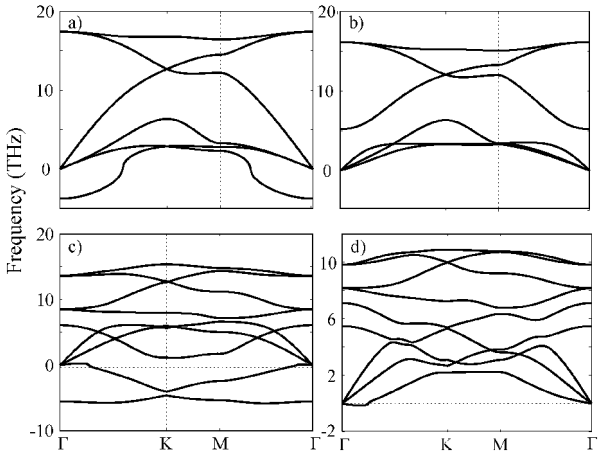

Fig. 3 Phonon dispersions of (a) planar and (b) buckled pristine silicene. (c) and (d) show the same for planar and buckled Ni-doped silicene, respectively.

modes, except for Ge. For the doped sheets, the buckling leads to hardening of the acoustic modes significantly as shown in Fig. 3(d).

Next, we study the effect of Ni doping on the electronic structures of these sheets. Fig. 4 shows the band structure and density of states (DOS) of planar and buckled pristine sheets. As it has been reported previously,[6] planar as well as buckled pristine Si sheets display semimetallic characteristics, because the π and π^* bands cross at the K point at the Fermi level E_F.[6] This is also evident from the DOS as there is a contribution of

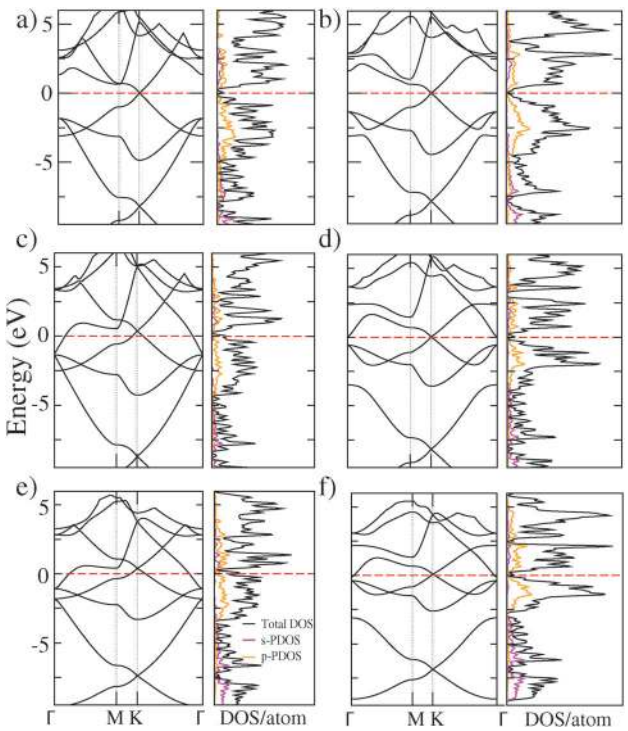

Fig. 4 Band structure and DOS of pristine sheets of (a) planar and (b) buckled Si, (c) planar and (d) buckled Ge, and (e) planar and (f) buckled Sn. The Fermi level, E_F is set at 0 eV.

the p orbitals (orange color) near the E_F for both planar and the buckled cases (Fig. 4(a) and (b)). In addition, the energy bands exhibit linear dispersion at the K point[6] similar to the case of graphene. Therefore, buckling does not influence linearity of the bands. However, in planar sheets of Ge and Sn, one of the conduction bands (at Γ point) falls below and gets occupied causing the shift in the Fermi level, which goes below the Dirac point. On the other hand, in the case of Ge and Sn buckled sheets, the conduction band becomes empty again and hence, the Dirac point occurs nearly at the Fermi level. Interestingly, when doped with Ni, the linear dispersion at the K point transforms to a quadratic one, as shown in Fig. 5(a). In the vicinity of the K point, the CBM falls below the VBM without any overlap. However, as we go from Si to Sn, these two bands come closer and eventually overlap. Furthermore, localized d orbitals of Ni form narrow bands near the E_F. The width of the Ni d bands decreases and the bands shift upwards from Si to Sn. This can also be observed from the DOS which shows that Ni d orbitals hybridize strongly with the p orbitals of the group-IV elements. The number of states significantly increases in the doped sheets, which will positively affect the conductivity of the sheets.

The localized narrow d bands of Ni suggest that correlations may play a significant role. It is known, that the position of Ni d-orbitals is inaccurately represented through PBE-GGA. Hence, additionally, we performed the electronic structure calculations of Ni-doped sheets using the LDA + U approach. However, there is no single value for the Coulombic repulsion parameter (U) in the literature. We found a range of U values starting from 4 eV to all the way upto 8 eV[35,36] depending upon the screening in the system. Therefore, we performed our calculations for both of these extreme values of U and found that the Ni d-orbitals get localized and shifted down depending upon the U value (Fig. 6). These shifts are minimal due to the metallic nature of the system. Therefore, overall, the band structure remains similar to the PBE-GGA results near the Fermi level.

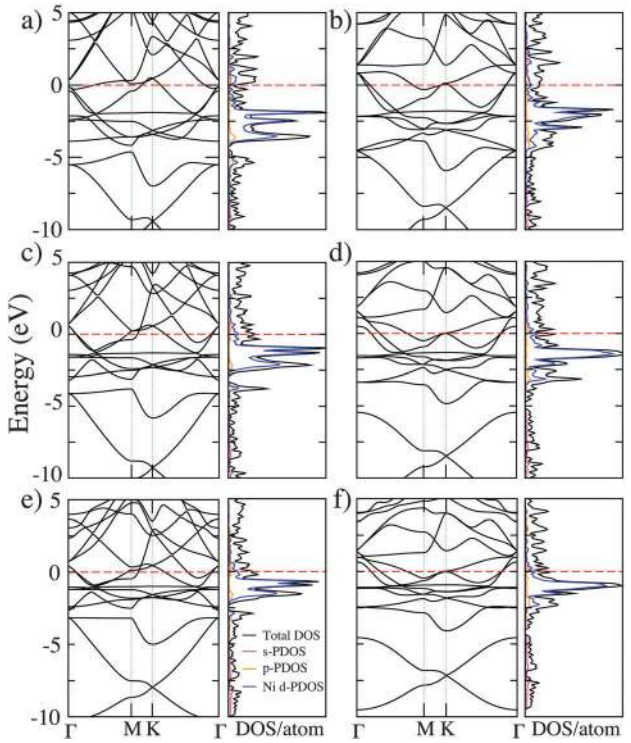

Fig. 5 Band structure and DOS of Ni-doped sheets of (a) planar and (b) buckled Si, (c) planar and (d) buckled Ge, (e) planar and (f) buckled Sn. The Fermi level E_F is set at 0 eV.

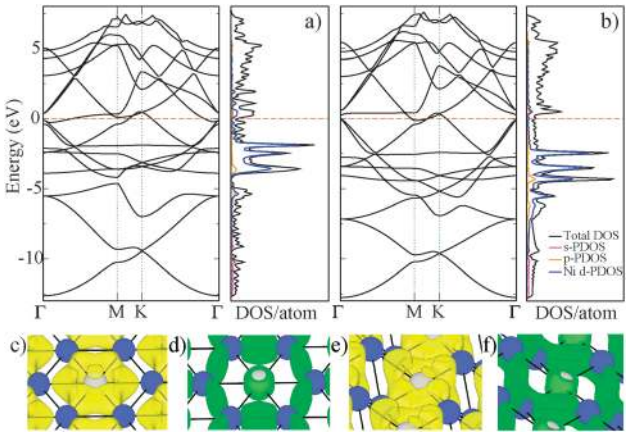

Fig. 6 Band structure and DOS of Ni-doped planar silicene calculated using (a) PBE-GGA and (b) LDA + U methods. Isosurfaces of charge accumulation (yellow) and depletion (green) are shown for Ni-doped planar (c) and (d) and buckled silicene (e) and (f), respectively.

Further studies have been done to assess the effect of different TM-atoms on the overall properties of these sheets. We investigated doping of these sheets with Fe and Co atoms which have nearly the same size as that of Ni atoms. Once again, the buckled structures are preferred over the planar ones. The phonon dispersions also show a qualitatively similar behavior as for the Ni case. The electronic properties do not change much as well. The Fe and Co doped sheets are also metallic, as shown in Fig. 7. Like Ni, the Fe and Co d-states lie deeper and therefore do not alter the electronic properties near the Fermi level. The magnetic moment in Fe and Co-doped sheets are quenched similar to the Ni-doped case.

In order to study the charge transfer, the charge accumulation and depletion (Fig. 6(c)–(f)) were calculated. There is a depletion of charge around the Si atoms and an accumulation of charge at Ni atoms implying charge transfer from Si to Ni. Bader charge[37,38] was calculated to obtain a quantitative measure of the charge transfer.

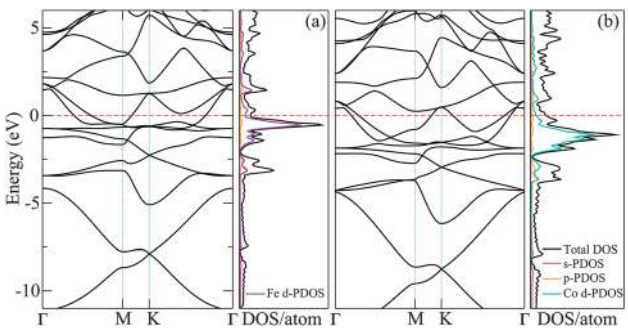

Fig. 7 Band structure and DOS of (a) Fe-doped and (b) Co-doped buckled silicene.

Consistent with the above analysis, a small amount of charge gets transferred from the Si sheet to the Ni atoms. An amount of 0.36 *e* and 0.38 *e* charge was found to be transferred from Si to Ni in the case of planar and buckled structures, respectively.

In summary, DFT based studies were performed on pristine and doped, planar and buckled Si, Ge, and Sn sheets. The energy differences, bond lengths, and buckling heights follow a systematic trend from Si to Sn. The increase in the energy differences for the doped sheets were larger, suggesting that the buckled sheets were further stabilized by Ni doping. Mechanical stability studies were also performed and a decreasing trend for the in-plane stiffness from Si to Sn has been obtained. The energy difference and the mechanical stability trends indicate that Ni stabilizes the sheets, with buckled sheets being more stable than the planar ones. Phonon dispersions show that the planar sheets are metastable and prefer transforming to stable buckled phases. Electronic band structure calculations showed that the doped sheets were more metallic than the pristine sheets. From the Bader charge analysis, the nature of bonding between Ni and the group IV elements is found to be metallic-covalent with charge transfer from group IV elements to Ni. Doping of these sheets with other TM atoms such as Fe and Co shows similar behavior as obtained for the Ni doped case.

Acknowledgements

AM and AKS would like to thank the Supercomputer Education and Research Centre and Materials Research Centre, IISc, for providing the required computational facilities necessary for the above work. AKS and AM acknowledge the support from ADA under NPMASS and DST nanomission. VK acknowledges the use of the computer facilities of the Center for Development of Advanced Computing (CDAC).

References

1 K. Novoselov, A. Geim, S. Morozov, D. Jiang, M. Katsnelson, I. Grigorieva, S. Dubonos and A. Firsov, *Nature*, 2005, **438**, 197–200.
2 A. Fleurence, R. Friedlein, T. Ozaki, H. Kawai, Y. Wang and Y. Yamada-Takamura, *Phys. Rev. Lett.*, 2012, **108**, 245501.
3 P. D. Padova, C. Quaresima, C. Ottaviani, P. M. Sheverdyaeva, P. Moras, C. Carbone, D. Topwal, B. Olivieri, A. Kara, H. Oughaddou, B. Aufray and G. L. Lay, *Appl. Phys. Lett.*, 2010, **96**, 261905.
4 P. D. Padova, C. Quaresima, B. Olivieri, P. Perfetti and G. L. Lay, *Appl. Phys. Lett.*, 2011, **98**, 081909.
5 K. Takeda and K. Shiraishi, *Phys. Rev. B: Condens. Matter Mater. Phys.*, 1994, **50**, 14916–14922.
6 S. Cahangirov, M. Topsakal, E. Aktürk, H. Şahin and S. Ciraci, *Phys. Rev. Lett.*, 2009, **102**, 236804.
7 E. Scalise, M. Houssa, G. Pourtois, B. Broek, V. Afanasev and A. Stesmans, *Nano Res.*, 2013, **6**, 19–28.
8 V. Kumar and Y. Kawazoe, *Phys. Rev. Lett.*, 2001, **87**, 045503.
9 V. Kumar and Y. Kawazoe, *Phys. Rev. Lett.*, 2003, **91**, 199901.
10 V. Kumar and Y. Kawazoe, *Phys. Rev. Lett.*, 2002, **88**, 235504.
11 V. Kumar and Y. Kawazoe, *Phys. Rev. Lett.*, 2003, **90**, 055502.
12 V. Kumar and Y. Kawazoe, *Phys. Rev. B: Condens. Matter Mater. Phys.*, 2002, **65**, 073404.
13 V. Kumar and Y. Kawazoe, *Appl. Phys. Lett.*, 2002, **80**, 859–861.
14 V. Kumar and Y. Kawazoe, *Appl. Phys. Lett.*, 2003, **83**, 2677–2679.
15 M. Ohara, K. Koyasu, A. Nakajima and K. Kaya, *Chem. Phys. Lett.*, 2003, **371**, 490–497.
16 V. Kumar, A. K. Singh and Y. Kawazoe, *Nano Lett.*, 2004, **4**, 677–681.
17 E. N. Esenturk, J. Fettinger and B. Eichhorn, *Chem. Commun.*, 2005, 247–249.
18 A. K. Singh, V. Kumar and Y. Kawazoe, *J. Mater. Chem.*, 2004, **14**, 555–563.
19 A. K. Singh, V. Kumar, T. M. Briere and Y. Kawazoe, *Nano Lett.*, 2002, **2**, 1243–1248.
20 A. K. Singh, T. M. Briere, V. Kumar and Y. Kawazoe, *Phys. Rev. Lett.*, 2003, **91**, 146802.
21 A. K. Singh, V. Kumar and Y. Kawazoe, *Phys. Rev. B: Condens. Matter Mater. Phys.*, 2004, **69**, 233406.
22 A. K. Singh, V. Kumar and Y. Kawazoe, *Phys. Rev. B: Condens. Matter Mater. Phys.*, 2004, **69**, 233406.
23 A. Kumar Singh, V. Kumar and Y. Kawazoe, *Eur. Phys. J. D*, 2005, **34**, 295–298.
24 A. K. Singh, V. Kumar and Y. Kawazoe, *Phys. Rev. B: Condens. Matter Mater. Phys.*, 2005, **71**, 075312.
25 W. Kohn and L. J. Sham, *Phys. Rev.*, 1965, **140**, A1133–A1138.
26 P. E. Blöchl, *Phys. Rev. B: Condens. Matter Mater. Phys.*, 1994, **50**, 17953–17979.
27 G. Kresse and D. Joubert, *Phys. Rev. B: Condens. Matter Mater. Phys.*, 1999, **59**, 1758–1775.
28 J. P. Perdew, K. Burke and M. Ernzerhof, *Phys. Rev. Lett.*, 1996, **77**, 3865–3868.
29 G. Kresse and J. Furthmüller, *Comput. Mater. Sci.*, 1996, **6**, 15–50.
30 G. Kresse and J. Furthmüller, *Phys. Rev. B: Condens. Matter Mater. Phys.*, 1996, **54**, 11169–11186.
31 H. J. Monkhorst and J. D. Pack, *Phys. Rev. B: Condens. Matter Mater. Phys.*, 1976, **13**, 5188–5192.
32 X. Gonze and J.-P. Vigneron, *Phys. Rev. B: Condens. Matter Mater. Phys.*, 1989, **39**, 13120–13128.
33 N. Y. Dzade, K. O. Obodo, S. K. Adjokatse, A. C. Ashu, E. Amankwah, C. Atiso, A. A. Bello, E. Igumbor, S. B. Nzabarinda, J. T. Obodo, A. O. Ogbuu, O. E. Femi, J. O. Udeigwe and U. V. Waghmare, *J. Phys.: Condens. Matter*, 2010, **22**, 375502.
34 E. Muñoz, A. K. Singh, M. A. Ribas, E. S. Penev and B. I. Yakobson, *Diamond Relat. Mater.*, 2010, **19**, 368–373.
35 S. L. Dudarev, G. A. Botton, S. Y. Savrasov, C. J. Humphreys and A. P. Sutton, *Phys. Rev. B: Condens. Matter Mater. Phys.*, 1998, **57**, 1505–1509.
36 V. I. Anisimov and O. Gunnarsson, *Phys. Rev. B: Condens. Matter Mater. Phys.*, 1991, **43**, 7570–7574.
37 R. F. W. Bader, *Atoms in Molecules: a Quantum Theory*, Oxford University Press, New York, 1990.
38 W. Tang, E. Sanville and G. Henkelman, *J. Phys.: Condens. Matter*, 2009, **21**, 084204.